J. Plasma Physics (2004), *vol.* 70, *part* 1, *pp.* 9–24.
DOI: 10.1017/S0022377803002459 Printed in the United Kingdom

Electron trajectories in a free-electron laser with helical wiggler, ion-channel guiding, and parallel/reversed axial magnetic field

MAHDI ESMAEILZADEH[1], HASSAN MEHDIAN[1] and JOSEPH E. WILLETT[2]

[1]Department of Physics, Teacher Training University, Tehran, Iran

[2]Department of Physics and Astronomy, University of Missouri-Columbia, Columbia, Missouri 65 211, USA
(willettje@missouri.edu)

(Received 20 April 2003 and accepted in revised form 29 May 2003)

Abstract. An analysis of electron trajectories in a helical magnetic wiggler with a uniform ion channel and a uniform axial magnetic field is presented. The axial field is considered in both the conventional and reversed directions. Equations for the transverse coordinates and velocities of a single relativistic electron in the combined ion electrostatic field and helical and axial magnetic fields are derived. A sixth-degree polynomial equation for the electron velocity and an equation for the function Φ (which determines the rate of change of axial velocity with energy) are derived. Results of some numerical calculations are presented to illustrate the effects of the electrostatic field and the axial magnetic field in each of the two configurations.

1. Introduction

The free-electron laser (FEL) is a high-intensity, continuously tunable source of coherent electromagnetic radiation for which many applications have been envisioned. These include a number of possible medical, industrial, communications, radar, controlled fusion, and basic scientific research applications. Freund and Antonsen [1] have presented a detailed discussion of FEL applications as well as some existing user facilities.

An axial magnetic guide field is often employed in the parallel-field configuration for which the cyclotron rotation of the electron beam is in the same direction as the rotation imposed by the helical wiggler magnetic field. It can also be employed in the reserved-field configuration for which the cyclotron rotation of the beam is in the direction opposite to the rotation imposed by the helical wiggler field. An experimental study shows that the output power and efficiency of the FEL in a reversed-field configuration can be higher than in the parallel-field configuration [2, 3]. An alternative guiding technique consists of passing the beam through an ion channel. Recent theoretical studies of the electron trajectories and gain in a FEL with ion-channel guiding indicate that this technique offers some distinct advantages [4, 5]. In the present paper electron trajectories in a FEL with helical

wiggler, ion-channel guiding, and an axial magnetic field in both the parallel-field and reversed-field configurations are studied.

The organization of this paper is as follows. In Sec. 2 the relativistic equation of motion for a single electron in the combined fields is solved for the transverse coordinates and velocities in the parallel-field configuration. A sixth-degree polynominal equation for the axial velocity is obtained by using conservation of energy. An equation is then derived for the function Φ which is used to determine the mass regimes. In Sec. 3 the orbital stability is investigated and stability conditions are derived. In Sec. 4 the electron trajectories and stability conditions for the reversed-field configuration are investigated. In Sec. 5 the results of a numerical study based on equations derived in Secs. 2, 3, and 4 are presented and discussed.

2. Electron trajectories and Φ (parallel-field configuration)

Consider a relativistic electron with rest mass m, charge e, and velocity $\boldsymbol{v}$ advancing in the positive z direction in a free-electron laser with helical wiggler field described by

$$\mathbf{B}_{\mathrm{w}} = B_{\mathrm{w}}(\hat{\mathbf{e}}_x \cos k_{\mathrm{w}} z + \hat{\mathbf{e}}_y \sin k_{\mathrm{w}} z), \tag{1}$$

where $k_{\mathrm{w}} = 2\pi/\lambda_{\mathrm{w}}$ is the wiggler wave number. The transverse electrostatic field generated by an ion channel can be written as

$$\mathbf{E}_{\mathrm{i}} = 2\pi e n_{\mathrm{i}}(x\hat{\mathbf{e}}_x + y\hat{\mathbf{e}}_y), \tag{2}$$

where n_{i} is the density of positive ions having charge $+e$. The equation of motion of the electron can be written as

$$\frac{d\mathbf{p}}{dt} = -e\left(\mathbf{E}_{\mathrm{i}} + \frac{1}{c}\mathbf{v} \times \mathbf{B}\right), \tag{3}$$

where

$$\mathbf{B} = \mathbf{B}_{\mathrm{w}} + \mathbf{B}_0, \tag{4}$$

and $\mathbf{B}_0 = B_0\hat{\mathbf{e}}_z$ is a uniform static magnetic field directed parallel to the wiggler axis (in the positive z direction). Using (1)–(4), the scalar equations of motion can be obtained as

$$\frac{d(m\gamma v_x)}{dt} = -2\pi e^2 n_{\mathrm{i}} x + \frac{eB_{\mathrm{w}}}{c} v_z \sin k_{\mathrm{w}} z - \frac{eB_0}{c} v_y, \tag{5}$$

$$\frac{d(m\gamma v_y)}{dt} = -2\pi e^2 n_{\mathrm{i}} y - \frac{eB_{\mathrm{w}}}{c} v_z \cos k_{\mathrm{w}} z + \frac{eB_0}{c} v_x, \tag{6}$$

$$\frac{d(m\gamma v_z)}{dt} = \frac{eB_{\mathrm{w}}}{c}(v_y \cos k_{\mathrm{w}} z - v_x \sin k_{\mathrm{w}} z), \tag{7}$$

where γ is the relativistic factor. The steady-state transverse electron displacements can be obtained by solving (5)–(7) ($v_z = v_\parallel =$ costant, $z = v_\parallel t$) in the form

$$x = \frac{\bar{\Omega}_{\mathrm{w}}\beta_\parallel}{k_{\mathrm{w}} c\left(\bar{\omega}_{\mathrm{i}}^2 - \beta_\parallel^2 + \bar{\Omega}_0\beta_\parallel\right)} \sin k_{\mathrm{w}} z, \tag{8}$$

$$y = -\frac{\bar{\Omega}_{\mathrm{w}}\beta_\parallel}{k_{\mathrm{w}} c\left(\bar{\omega}_{\mathrm{i}}^2 - \beta_\parallel^2 + \bar{\Omega}_0\beta_\parallel\right)} \cos k_{\mathrm{w}} z, \tag{9}$$

https://doi.org/10.1017/S0022377803002459 Published online by Cambridge University Press

where $\bar{\Omega}_{\rm w} \equiv \Omega_{\rm w}/ck_{\rm w}$, $\Omega_{\rm w} \equiv eB_{\rm w}/\gamma mc$, $\beta_\parallel \equiv v_\parallel/c$, $\bar{\omega}_{\rm i} \equiv \omega_{\rm i}/ck_{\rm w}$, $\omega_{\rm i}^2 \equiv 2\pi e^2 n_{\rm i}/\gamma m$, $\bar{\Omega}_0 \equiv \Omega_0/ck_{\rm w}$, and $\Omega_0 \equiv eB_0/\gamma mc$. Hence, the electron trajectory is a perfect helix with its axis coincident with the free-electron laser axis. Using (8) and (9), the normalized transverse electron velocities can be written as

$$\beta_x = \frac{\bar{\Omega}_{\rm w}\beta_\parallel^2}{\bar{\omega}_{\rm i}^2 - \beta_\parallel^2 + \bar{\Omega}_0\beta_\parallel} \cos k_{\rm w} z, \tag{10}$$

$$\beta_y = \frac{\bar{\Omega}_{\rm w}\beta_\parallel^2}{\bar{\omega}_{\rm i}^2 - \beta_\parallel^2 + \bar{\Omega}_0\beta_\parallel} \sin k_{\rm w} z, \tag{11}$$

where $\beta_x \equiv v_x/c$ and $\beta_y \equiv v_y/c$. These orbits show a resonant enhancement in the magnitude of the transverse velocities when

$$\bar{\omega}_{\rm i}^2 - \beta_\parallel^2 + \bar{\Omega}_0\beta_\parallel \simeq 0. \tag{12}$$

The foregoing analysis contains two important cases: if $\bar{\Omega}_0$ is set equal to zero (eliminating the axial magnetic field) the transverse velocities become [1]

$$\beta_x = \frac{\bar{\Omega}_{\rm w}\beta_\parallel^2}{\bar{\omega}_{\rm i}^2 - \beta_\parallel^2} \cos k_{\rm w} z, \tag{13}$$

$$\beta_y = \frac{\bar{\Omega}_{\rm w}\beta_\parallel^2}{\bar{\omega}_{\rm i}^2 - \beta_\parallel^2} \sin k_{\rm w} z, \tag{14}$$

and the resonant condition becomes

$$\bar{\omega}_{\rm i} \simeq \beta_\parallel, \tag{15}$$

for a helical wiggler with ion-channel guiding only. If $\bar{\omega}_{\rm i}$ is set equal to zero (eliminating the ion channel), the transverse velocities become

$$\beta_x = \frac{\bar{\Omega}_{\rm w}\beta_\parallel}{\bar{\Omega}_0 - \beta_\parallel} \cos k_{\rm w} z, \tag{16}$$

$$\beta_y = \frac{\bar{\Omega}_{\rm w}\beta_\parallel}{\bar{\Omega}_0 - \beta_\parallel} \sin k_{\rm w} z, \tag{17}$$

and the resonant condition becomes

$$\bar{\Omega}_0 \simeq \beta_\parallel, \tag{18}$$

for a helical wiggler with axial magnetic field only.

The normalized axial velocity $\beta_\parallel$ can be obtained from the conservation of energy using (10) and (11). A sixth-degree polynomial equation,

$$\beta_\parallel^2 \left[1 + \frac{\bar{\Omega}_{\rm w}^2\beta_\parallel^2}{\left(\bar{\omega}_{\rm i}^2 - \beta_\parallel^2 + \bar{\Omega}_0\beta_\parallel\right)^2}\right] = 1 - \gamma^{-2}, \tag{19}$$

is thereby obtained. There are in general six solutions for $\beta_\parallel$ for each set of parameters; of these only the three for which $\beta_\parallel > 0$ (corresponding to advance of the electron in the positive z direction) will be employed. Implicit differentiation of

https://doi.org/10.1017/S0022377803002459 Published online by Cambridge University Press

(19) yields

$$\frac{d\beta_\parallel}{d\gamma} = \frac{1}{\gamma\gamma_\parallel^2\beta_\parallel}\Phi, \tag{20}$$

where

$$\Phi = 1 - \frac{\bar{\Omega}_\mathrm{w}^2\beta_\parallel^2\left[\left(\bar{\Omega}_0\beta_\parallel + \bar{\omega}_\mathrm{i}^2\right)\gamma_\parallel^2 + \bar{\omega}_\mathrm{i}^2\right]}{\left(\bar{\omega}_\mathrm{i}^2 - \beta_\parallel^2 + \bar{\Omega}_0\beta_\parallel\right)^3 + \bar{\Omega}_\mathrm{w}^2\beta_\parallel^2\left(\bar{\Omega}_0\beta_\parallel + 2\bar{\omega}_\mathrm{i}^2\right)} \tag{21}$$

and $\gamma_\parallel = (1-\beta_\parallel^2)^{-1/2}$. Equation (21) determines the rate of variation of the axial velocity with electron energy. If $\bar{\Omega}_0$ is set equal to zero (eliminating the axial magnetic field), (21) becomes

$$\Phi = 1 - \frac{(1+\gamma_\parallel^2)\bar{\Omega}_\mathrm{w}^2\bar{\omega}_\mathrm{i}^2\beta_\parallel^2}{\left(\bar{\omega}_\mathrm{i}^2 - \beta_\parallel^2\right)^3 + 2\bar{\Omega}_\mathrm{w}^2\bar{\omega}_\mathrm{i}^2\beta_\parallel^2}, \tag{22}$$

for a helical wiggler with ion-channel guiding only. If $\bar{\omega}_\mathrm{i}$ is set equal to zero (eliminating the ion channel), (21) becomes

$$\Phi = 1 - \frac{\gamma_\parallel^2\bar{\Omega}_0\bar{\Omega}_\mathrm{w}^2}{(\bar{\Omega}_0 - \beta_\parallel)^3 + \bar{\Omega}_0\bar{\Omega}_\mathrm{w}^2}, \tag{23}$$

for a helical wiggler with axial magnetic field guiding only. The analysis in the absence of an ion channel was first carried out by Friedland [6] using the wiggler frame and has been discussed in detail by Freund and Antonsen [1]. Equations (16), (18), and (23) can be shown to be equivalent to the corresponding equations derived in the wiggler frame.

3. Stability of electron orbits

The wiggler frame (a coordinate frame which rotates with the wiggler field) is defined by basis vectors:

$$\hat{\mathbf{e}}_1 = \hat{\mathbf{e}}_x \cos k_\mathrm{w} z + \hat{\mathbf{e}}_y \sin k_\mathrm{w} z, \tag{24}$$

$$\hat{\mathbf{e}}_2 = -\hat{\mathbf{e}}_x \sin k_\mathrm{w} z + \hat{\mathbf{e}}_y \cos k_\mathrm{w} z, \tag{25}$$

$$\hat{\mathbf{e}}_3 = \hat{\mathbf{e}}_z. \tag{26}$$

In this frame, the scalar equations of motion can be written as

$$\frac{dv_1}{dt} = -\omega_\mathrm{i}^2 x_1 - (\Omega_0 - k_\mathrm{w} v_3)v_2, \tag{27}$$

$$\frac{dv_2}{dt} = -\omega_\mathrm{i}^2 x_2 + (\Omega_0 - k_\mathrm{w} v_3)v_1 - \Omega_\mathrm{w} v_3, \tag{28}$$

$$\frac{dv_3}{dt} = \Omega_\mathrm{w} v_2. \tag{29}$$

Using (24)–(26), the velocities v_1, v_2, and v_3 in the wiggler frame can be obtained as

$$v_1 = \dot{x}_1 - k_\mathrm{w} v_3 x_2, \tag{30}$$

$$v_2 = \dot{x}_2 + k_\mathrm{w} v_3 x_1, \tag{31}$$

$$v_3 = \dot{x}_3, \tag{32}$$

https://doi.org/10.1017/S0022377803002459 Published online by Cambridge University Press

where dots indicate differentiation with respect to time. The steady-state solution of (27)–(29) can be obtained by setting the derivatives of these equations equal to zero. Then by using (30)–(32) we have

$$v_{10} = \frac{c\bar{\Omega}_{\mathrm{w}}\beta_{\parallel}^2}{\bar{\omega}_{\mathrm{i}}^2 - \beta_{\parallel}^2 + \bar{\Omega}_0\beta_{\parallel}}, \tag{33}$$

$$v_{20} = 0, \tag{34}$$

$$v_{30} = v_{\parallel} = c\beta_{\parallel} = \text{constant}, \tag{35}$$

for electron velocity and

$$x_{10} = 0, \tag{36}$$

$$x_{20} = -\frac{\bar{\Omega}_{\mathrm{w}}\beta_{\parallel}}{k_{\mathrm{w}}\left(\bar{\omega}_{\mathrm{i}}^2 - \beta_{\parallel}^2 + \bar{\Omega}_0\beta_{\parallel}\right)}, \tag{37}$$

$$x_{30} = v_{30}t = c\beta_{\parallel}t, \tag{38}$$

for electron position, where subscript 0 indicates steady state.

The stability of these steady-state solutions can be examined by considering small perturbations $x_1 = \delta x_1$, $x_2 = x_{20} + \delta x_2$, $\dot{x}_1 = \delta\dot{x}_1$, $\dot{x}_2 = \delta\dot{x}_2$, and $\dot{x}_3 = v_{\parallel} + \delta\dot{x}_3$. Eliminating v_1, v_2, and v_3 in the orbital equations (27)–(29) by using (30)–(32) and their time derivatives, and then expanding to first order in the perturbed position and its time derivative, we obtain

$$\delta\ddot{x}_1 = c_1\delta x_1 + c_2\delta\dot{x}_2 + c_3\delta\ddot{x}_3, \tag{39}$$

$$\delta\ddot{x}_2 = c_1\delta x_2 - c_2\delta\dot{x}_1 + c_4\delta\ddot{x}_3, \tag{40}$$

$$\delta\ddot{x}_3 = c_5\delta\dot{x}_2 + c_6\delta x_1, \tag{41}$$

where

$$\begin{aligned}
c_1 &= -\left(\bar{\omega}_{\mathrm{i}}^2 - \beta_{\parallel}^2 + \bar{\Omega}_0\beta_{\parallel}\right)c^2k_{\mathrm{w}}^2,\\
c_2 &= -(\bar{\Omega}_0 - 2\beta_{\parallel})ck_{\mathrm{w}},\\
c_3 &= x_{20}k_{\mathrm{w}}^2,\\
c_4 &= -[\bar{\Omega}_{\mathrm{w}} + (\bar{\Omega}_0 - 2\beta_{\parallel})x_{20}k_{\mathrm{w}}]ck_{\mathrm{w}},\\
c_5 &= \bar{\Omega}_{\mathrm{w}}ck_{\mathrm{w}},\\
c_6 &= \bar{\Omega}_{\mathrm{w}}\beta_{\parallel}c^2k_{\mathrm{w}}^2.
\end{aligned} \tag{42}$$

Differentiating (39) and (40) with respect to time and using (41) and its time derivative yields

$$\delta\ddot{x}_1 = (c_1 + c_3c_6)\delta\dot{x}_1 + (c_2 + c_3c_5)\delta\ddot{x}_2, \tag{43}$$

$$\delta\ddot{x}_2 = (c_1 + c_4c_5)\delta\dot{x}_2 - c_2\delta\ddot{x}_1 + c_4c_6\delta x_1. \tag{44}$$

The stability of electron orbits may be investigated as follows. All displacements oscillate with the same frequency ω and are represented by

$$\delta x_j = A_j\, e^{i\omega t}, \quad j = 1, 2. \tag{45}$$

https://doi.org/10.1017/S0022377803002459 Published online by Cambridge University Press

Substituting (45) into (43) and (44) yields

$$i\omega(\omega^2 + c_1 + c_3c_6)A_1 - (\omega^2 c_2 + c_3c_5)A_2 = 0, \tag{46}$$

$$(\omega^2 c_2 + c_4c_6)A_1 + i\omega(\omega^2 + c_1 + c_4c_5)A_2 = 0. \tag{47}$$

The above homogeneous linear equations have a non-trivial solution only if the determinant of the coefficients of unknowns A_1, A_2 vanishes; thus

$$\omega^4 + b\omega^2 + c = 0, \tag{48}$$

where

$$b \equiv 2c_1 - c_2^2 + c_4c_5 + c_3c_6 - c_2c_3c_5 \tag{49}$$

and

$$c \equiv (c_1 + c_3c_6)(c_1 + c_4c_5) - c_4c_6(c_2 + c_3c_5). \tag{50}$$

Equation (48) is the characteristic equation of the system and is quadratic in ω^2. Hence the system will be stable if both roots of (48) are real and positive. Therefore the stability conditions for electron orbits can be written as

$$\begin{aligned} b^2 - 4c &> 0, \\ b &< 0, \\ c &> 0. \end{aligned} \tag{51}$$

4. Reversed-field configuration

In this section we study the electron trajectories in a FEL with helical wiggler, ion-channel guiding, and axial magnetic field in the reversed-field configuration. With axial magnetic field $\mathbf{B}_0$ replaced by $-B_0\hat{\mathbf{e}}_z$ in (4), the scalar equations of motion can be written as

$$\frac{dv_x}{dt} = -\omega_{\mathrm{i}}^2 x + \Omega_{\mathrm{w}} v_z \sin k_{\mathrm{w}} z + \Omega_0 v_y, \tag{52}$$

$$\frac{dv_y}{dt} = -\omega_{\mathrm{i}}^2 y + \Omega_{\mathrm{w}} v_z \cos k_{\mathrm{w}} z - \Omega_0 v_x, \tag{53}$$

$$\frac{dv_z}{dt} = \Omega_{\mathrm{w}}(v_y \cos k_{\mathrm{w}} z - v_x \sin k_{\mathrm{w}} z). \tag{54}$$

Following the procedure of the steady-state solution, the transverse velocity can be obtained in the form

$$\beta_x = \frac{\bar{\Omega}_{\mathrm{w}}\beta_\parallel^2}{\bar{\omega}_{\mathrm{i}}^2 - \beta_\parallel^2 - \bar{\Omega}_0\beta_\parallel} \cos k_{\mathrm{w}} z, \tag{55}$$

$$\beta_y = \frac{\bar{\Omega}_{\mathrm{w}}\beta_\parallel^2}{\bar{\omega}_{\mathrm{i}}^2 - \beta_\parallel^2 - \bar{\Omega}_0\beta_\parallel} \sin k_{\mathrm{w}} z. \tag{56}$$

The above equations show a resonant enhancement in the magnitude of the transverse velocity for the reversed-field configuration when

$$\bar{\omega}_{\mathrm{i}}^2 - \beta_\parallel^2 - \bar{\Omega}_0\beta_\parallel \simeq 0. \tag{57}$$

https://doi.org/10.1017/S0022377803002459 Published online by Cambridge University Press

If $\bar{\omega}_{\mathrm{i}}$ is set equal to zero, the components of transverse velocity become

$$\beta_x = -\frac{\bar{\Omega}_{\mathrm{w}}\beta_{\parallel}}{\bar{\Omega}+\beta_{\parallel}}\cos k_{\mathrm{w}}z, \tag{58}$$

$$\beta_y = -\frac{\bar{\Omega}_{\mathrm{w}}\beta_{\parallel}}{\bar{\omega}_0+\beta_{\parallel}}\sin k_{\mathrm{w}}z. \tag{59}$$

In contradistinction to (16) and (17) for the parallel-field configuration, (58) and (59) do not predict any resonance condition for the reversed-field configuration in this case ($\bar{\omega}_{\mathrm{i}} = 0$).

The axial velocity for the reversed-field configuration can be obtained from conservation of energy. Equations (55) and (56) yield

$$\beta_{\parallel}^2\left[1+\frac{\bar{\Omega}_{\mathrm{w}}^2\beta_{\parallel}^2}{\left(\bar{\omega}_{\mathrm{i}}^2+\beta_{\parallel}^2-\bar{\Omega}_0\beta_{\parallel}\right)^2}\right] = 1-\gamma^{-2}. \tag{60}$$

The function Φ in the reversed-field configuration is then obtained in the form

$$\Phi = 1-\frac{\bar{\Omega}_{\mathrm{w}}^2\beta_{\parallel}^2\left[\left(\bar{\omega}_{\mathrm{i}}^2-\bar{\Omega}_{\parallel}\beta_0\right)\gamma_{\parallel}^2+\bar{\omega}_{\parallel}^2\right]}{\left(\bar{\omega}_{\mathrm{i}}^2-\beta_{\parallel}^2-\bar{\Omega}_0\beta_{\parallel}\right)^3+\bar{\Omega}_{\mathrm{w}}^2\beta_{\parallel}^2\left(2\bar{\omega}_{\mathrm{i}}^2-\bar{\Omega}_0\beta_{\parallel}\right)}. \tag{61}$$

As we see in (59)–(61), these equation are the same as those of the parallel-field configuration with $\bar{\Omega}_0$ replaced by $-\bar{\Omega}_0$. If we replace $\beta_{\parallel}$ by $-\beta_{\parallel}$ in those equations in Sec. 2, we obtain the same results as replacing $\bar{\Omega}_0$ by $-\bar{\Omega}_0$. Therefore, a backward electron beam propagating ($\beta_{\parallel} < 0$) in a free-electron laser (parallel-field configuration) with and without ion-channel guiding can be considered as a forward electron beam propagating with a reversed-axial magnetic field configuration.

The stability condition for electron orbits in the reversed-field configuration can be obtained as in Sec. 3 and the results are the same as (51) with $\bar{\Omega}_0$ replaced by $-\bar{\Omega}_0$ in c_j ($j = 1, 2, \ldots, 6$).

5. Numerical results and discussion

A numerical study of steady-state relativistic electron trajectories in a FEL with a helical wiggler magnetic field in the presence of an axial magnetic field and ion channel has been made. The normalized (bulk) axial velocity $\beta_{\parallel}$ and the function Φ (which is used to determine the rate of change of $\beta_{\parallel}$ with electron energy and to determine the mass regimes) have been computed by using (19) and (21) for the conventional parallel-field configuration and (60) and (61) for the reversed-field configuration. The electron energy was taken to be 1 MeV ($\gamma = 2.957$) and the normalized wiggler magnetic field $\bar{\Omega}_{\mathrm{w}}$ was taken to be 0.05 except in one case for the reversed field when it was taken to be 0.45.

5.1. Conventional parallel-field configuration

In Figs 1–3, $\beta_{\parallel}$ is shown as a function of the normalized frequency of the beam-guiding device for the parallel-field configuration. Figure 1 shows $\beta_{\parallel}$ as a function of the normalized ion-channel frequency $\bar{\omega}_{\mathrm{i}}$ in the presence of an axial magnetic field when it is held constant with $\bar{\Omega}_0 = 0.5$. As this figure shows there are two

https://doi.org/10.1017/S0022377803002459 Published online by Cambridge University Press

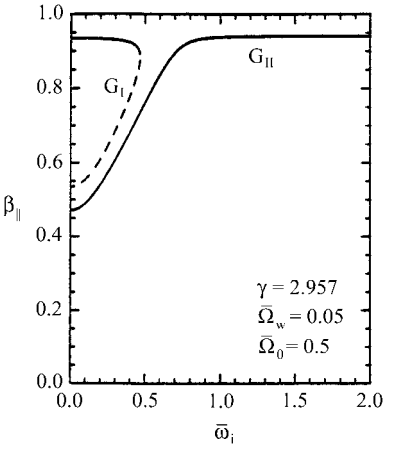

Figure 1. Normalized axial velocity versus normalized ion-channel frequency with no axial magnetic field.

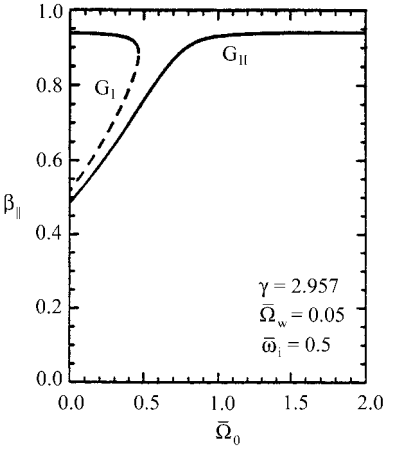

Figure 2. Normalized axial velocity versus normalized conventional axial magnetic field with ion channel.

groups of orbits. Group I (G_I) and Group II (G_{II}) orbits are determined by

$$\bar{\omega}_i^2 < \beta_\parallel(\beta_\parallel - \bar{\Omega}_0) \tag{62}$$

and

$$\bar{\omega}_i^2 > \beta_\parallel(\beta_\parallel - \bar{\Omega}_0) \tag{63}$$

respectively. The dashed line indicates an unstable branch of Group I orbits for which the stability condition (51) is not satisfied. From (62) we see that for stable and unstable branches of Group I orbits, $\beta_\parallel$ must be greater than $\bar{\Omega}_0$ (=0.5), which agrees with Fig. 1. Figure 2 shows $\beta_\parallel$ as a function of the normalized axial magnetic field $\bar{\Omega}_0$ in the presence of an ion channel when it is held constant with $\bar{\omega}_i = 0.5$. In

https://doi.org/10.1017/S0022377803002459 Published online by Cambridge University Press

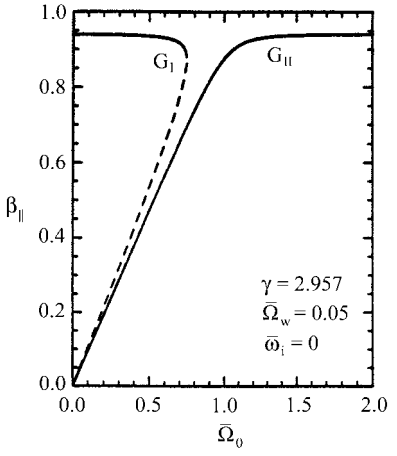

Figure 3. Normalized axial velocity versus normalized conventional axial magnetic field with no ion channel.

this figure Group I and Group II orbits are determined by

$$\bar{\Omega}_0 < \left(\beta_\parallel - \bar{\omega}_i^2/\beta_\parallel\right) \tag{64}$$

and

$$\bar{\Omega}_0 > \left(\beta_\parallel - \bar{\omega}_i^2/\beta_\parallel\right) \tag{65}$$

respectively. The dashed line indicates the unstable branch of Group I orbits for which the stability condition (51) is not satisfied. Figures 1 and 2 are similar but are not identical. Figure 3 shows $\beta_\parallel$ as a function of $\bar{\Omega}_0$ in the absence of an ion channel. Group I and Group II are determined by $\bar{\Omega}_0 < \beta_\parallel$ and $\bar{\Omega}_0 > \beta_\parallel$, respectively. The dashed line indicates the unstable branch of Group I orbits for which the stability condition (51) is not satisfied. The results of this simplified case ($\bar{\omega}_i = 0$) agree with the results of previously published papers [1, 6, 7]. As is shown in Figs 1–3 for stable Group I orbits, $\beta_\parallel$ decreases gradually with increasing guiding frequency until the curve terminates at the point of orbit instability. For Group II orbits, $\beta_\parallel$ increases monotonically approaching a limit as the guiding frequency approaches infinity and the transverse velocity approaches zero. As Figs 1 and 2 show, for combined beam-guiding devices, $\beta_\parallel$ for unstable Group I orbits and Group II orbits never approaches zero even when the guiding frequency approaches zero.

In Figs 4–6, Φ is shown as a function of the normalized frequency of the beam-guiding device. Figure 4 shows Φ as a function of $\bar{\omega}_i$ in the presence of an axial magnetic field when it is held constant with $\bar{\Omega}_0 = 0.5$. For stable Group I orbits, Φ increases monotonically and exhibits a singularity at the transition to orbit instability. Since the axial velocity increases with increasing energy, these orbits correspond to a positive-mass regime. For Group II orbits there are two mass regimes, i.e. a negative-mass regime where $\Phi < 0$ and a positive-mass regime where $\Phi > 0$. The existence of the negative-mass regime is interesting because the axial velocity will increase with decreasing electron-beam energy. Figure 5 shows Φ as a function of $\bar{\Omega}_0$ for stable Group I orbits and Group II orbits in the presence of an ion channel when it is held constant with $\bar{\omega}_i = 0.5$. Figure 6 shows Φ as a function

https://doi.org/10.1017/S0022377803002459 Published online by Cambridge University Press

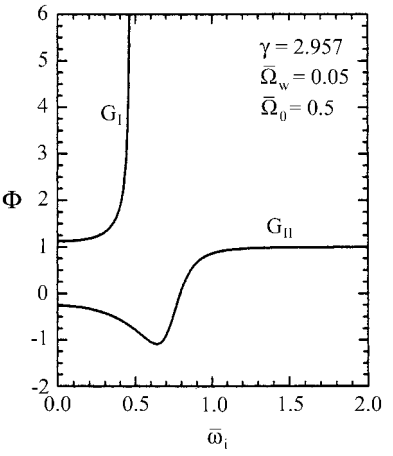

Figure 4. Function Φ versus normalized ion-channel frequency with conventional axial magnetic field.

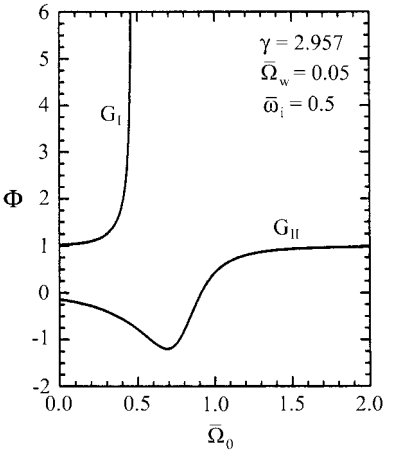

Figure 5. Function Φ versus normalized conventional axial magnetic field with ion channel.

of $\bar{\Omega}_0$ for stable Group I orbits and Group II orbits in the absence of an ion channel. Figures 1, 2, and 3 are similar but are not identical.

5.2. Reversed-field configuration

In Figs 5–7, $\beta_\parallel$ is shown as a function of the normalized frequency of the beam-guiding device for the reversed-axial magnetic field configuration. Figure 7 shows $\beta_\parallel$ as a function of $\bar{\omega}_i$ in the presence of a constant reversed field with $\bar{\Omega}_0 = 0.5$. Group I and Group II orbits are determined by

$$\bar{\omega}_i^2 < \beta_\parallel(\beta_\parallel + \bar{\Omega}_0) \tag{66}$$

and

$$\bar{\omega}_i^2 > \beta_\parallel(\beta_\parallel + \bar{\Omega}_0) \tag{67}$$

https://doi.org/10.1017/S0022377803002459 Published online by Cambridge University Press

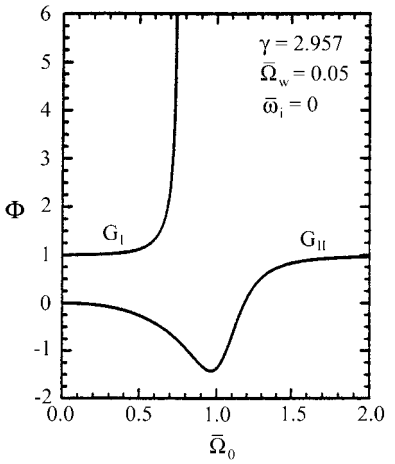

Figure 6. Function Φ versus normalized conventional axial magnetic field with no ion channel.

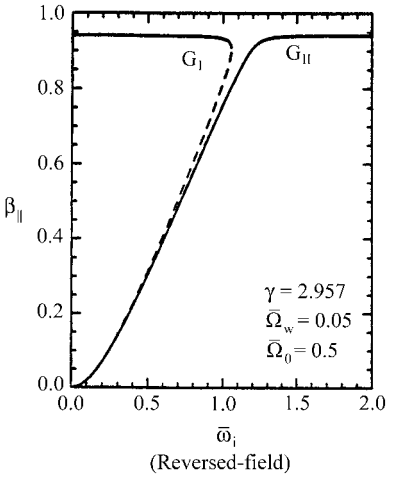

Figure 7. Normalized axial velocity versus normalized ion-channel frequency with reversed axial magnetic field.

respectively. As Figs 1 and 7 show, the main difference between parallel and reversed fields is that for unstable Group I and Group II orbits, $\beta_\parallel$ starts increasing from around 0.5 with increasing $\bar{\omega}_i$ (and constant $\bar{\Omega}_0$) for the parallel field and starts increasing from zero for the reversed field. Therefore, conservation of energy requires that for small $\bar{\omega}_i$, the transverse velocity is greater for a reversed field than a parallel field. Figures 8 and 9 show $\beta_\parallel$ as a function of $\bar{\Omega}_0$ in the presence of an ion channel held constant with $\bar{\omega}_i = 0.5$ for the reversed field. As shown in Fig. 8 for stable Group I orbits, $\beta_\parallel$ is relatively constant over the entire indicated range of $\bar{\Omega}_0$. For unstable Group I orbits and Group II orbits, $\beta_\parallel$ decreases monotonically approaching zero as $\bar{\Omega}_0$ approaches infinity and the transverse velocity approaches its maximum value. Figure 9 is the same as Fig. 8, but we have set the normalized

https://doi.org/10.1017/S0022377803002459 Published online by Cambridge University Press

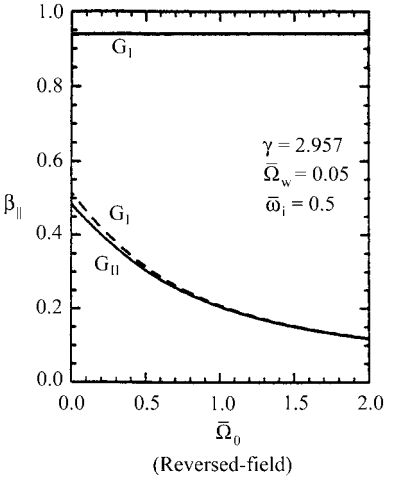

Figure 8. Normalized axial velocity versus normalized reversed axial magnetic field with ion channel.

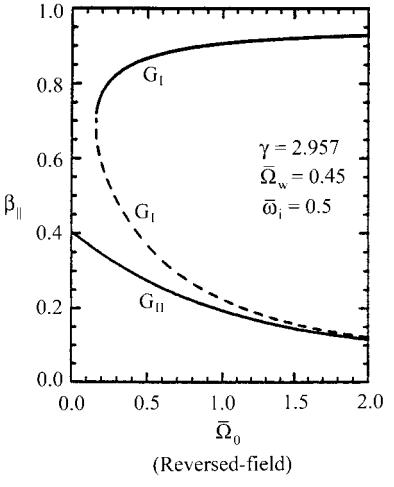

Figure 9. Normalized axial velocity versus normalized reversed axial magnetic field with ion channel.

wiggler magnetic field $\bar{\Omega}_w = 0.45$ to show complete stable and unstable branches of Group I orbits. Group I and Group II orbits for Figs 8 and 9 are determined by

$$\bar{\Omega}_0 > \frac{\bar{\omega}_i^2}{\beta_{\|}} - \beta_{\|} \tag{68}$$

and

$$\bar{\Omega}_0 < \frac{\bar{\omega}_i^2}{\beta_{\|}} - \beta_{\|} \tag{69}$$

https://doi.org/10.1017/S0022377803002459 Published online by Cambridge University Press

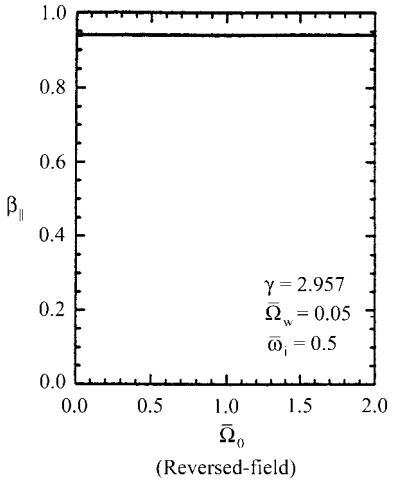

Figure 10. Normalized axial velocity versus normalized reversed axial magnetic field with no ion channel.

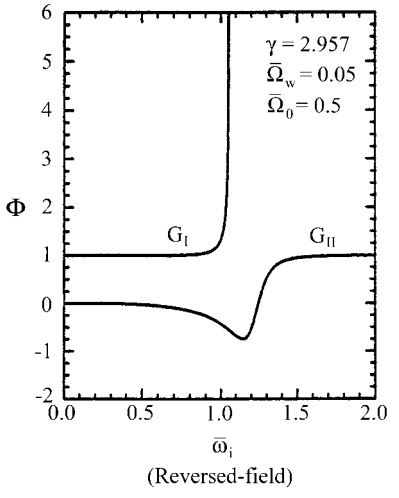

Figure 11. Function Φ versus normalized ion-channel frequency with reversed axial magnetic field.

respectively. Figure 10 shows $\beta_\parallel$ as a function of $\bar{\Omega}_0$ in the absence of an ion channel. This figure shows that there is one class of orbits for this reversed configuration and it is stable. As mentioned in Sec. 4 for this case of a reversed field there is no resonant enhancement in the wiggler-induced transverse velocity (cf. (58) and (59)). As shown in this figure, $\beta_\parallel$ is relatively constant over the entire indicated range of $\bar{\Omega}_0$.

In Figs 11–14 the function Φ is shown as a function of the normalized beam-device frequency for the reversed-field configuration. Figure 11 shows Φ as a function of $\bar{\omega}_i$ in the presence of a constant axial magnetic field with $\bar{\Omega}_0 = 0.5$ for stable Group I

https://doi.org/10.1017/S0022377803002459 Published online by Cambridge University Press

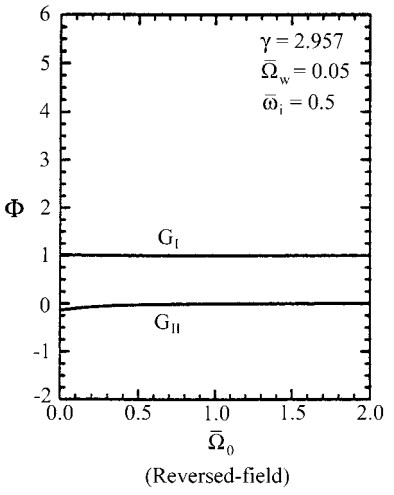

Figure 12. Function Φ versus normalized reversed axial magnetic field with ion channel.

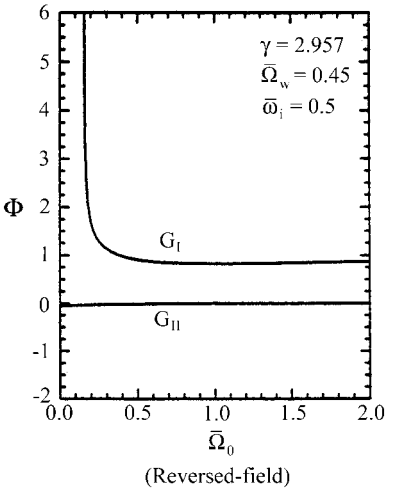

Figure 13. Function Φ versus normalized reversed axial magnetic field with ion channel and stronger wiggler field.

orbits and Group II orbits. As shown in this figure, there is a positive-mass regime for Group I orbits and there are negative- and positive-mass regimes for Group II orbits. Figures 12 and 13 show Φ as a function of $\bar{\Omega}_0$ in the presence of an ion channel when it is held constant with $\bar{\omega}_i = 0.5$ for stable Group I and Group II orbits. As shown in Fig. 12 for stable Group I orbits Φ is relatively constant and equal to 1; for Group II orbits Φ is relatively constant and approximately equal to zero. Therefore, for Group II orbits, with a good approximation there is a zero-mass regime in which only the transverse electron velocity increases with increasing energy. In Fig. 13 we have set $\bar{\Omega}_w = 0.45$, and as shown in this figure for Group II orbits there is an approximately zero-mass regime; for Group I orbits Φ decreases monotonically

https://doi.org/10.1017/S0022377803002459 Published online by Cambridge University Press

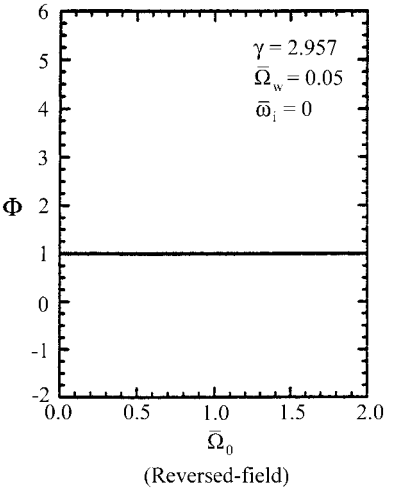

Figure 14. Function Φ versus normalized reversed axial magnetic field with no ion channel.

from infinity (singularity at the transition to orbit instability) and approaches a limit near 1 as $\bar{\Omega}_0$ approaches infinity. Figure 14 shows Φ as a function of $\bar{\Omega}_0$ is the absence of an ion channel for the reversed configuration. As shown in this figure Φ is nearly constant ($\simeq$1) over the entire indicated range of $\bar{\Omega}_0$. Therefore, for this simplified case ($\bar{\omega}_i = 0$) there is only one class of mass regime and it is positive.

It is important to note that the electric fields due to the ion channel and the beam electrons may give rise to a kinetic energy spread across the beam. The relativistic factor γ must satisfy the equation

$$\frac{d}{dt}\left[\gamma - \frac{\pi e^2 r^2}{c^2 m}(n_b - n_i)\right] = 0, \tag{70}$$

where r is the distance from the axis. Thus, the change in γ from the centre ($r = 0$) to the edge ($r = R_b$) of the beam is given by

$$\Delta\gamma = \pi e^2 R_b^2 (n_b - n_i)/mc^2. \tag{71}$$

This implies that when the ion density n_i is much less than the beam electron density n_e, the fractional variation of γ for $n_e = 10^{12}$ cm^{-3} is

$$\Delta\gamma/\gamma = 0.885\, R_b^2/\gamma \tag{72}$$

with R_b in cm. The deleterious effects of energy spread may be reduced with sufficiently small R_b and/or large γ, e.g. $\Delta\gamma/\gamma = 1.2 \times 10^{-2}$ if $R_b = 0.2$ cm and $\gamma = 2.957$. The restriction on R_b^2/γ decreases as n_i is increased and vanished when $n_i = n_b$. This suggests that another advantage of the ion core is in reducing the energy spread. The electron trajectories remain helical when $\Delta\gamma$ is negligible and the present analysis remains valid. It should also be noted that the self-electric and self-magnetic fields tend to cancel each other at sufficiently large γ. At small γ their effects may be approximated by appropriately chosen effective ion density and wiggler field [8].

The use of ion-channel guiding in a FEL offers a number of possible advantages. It has been suggested that this technique would be more economical, would permit

https://doi.org/10.1017/S0022377803002459 Published online by Cambridge University Press

higher beam currents and enhanced growth rate, and would tend to suppress instabilities, emittance growth, and energy spread across the beam (see [5] and references cited therein). Caporasa et al. reported in 1986 the first successful use of ion-channel guiding [9]. It was employed to transport a 10-kA electron beam through an advanced test accelerator. Ozaki et al. carried out FEL experiments using an ion channel in 1989 with only modest success. Their subsequent experiments, carried out after extending the wiggler and reconfiguring the rf input, showed a vast improvement in FEL performance [10]. A definitive test of the feasibility of using ion-channel guiding in a FEL remains a challenging experimental task which is yet to be performed.

References

[1] Freund, H. P. and Antonsen, J. M. Jr 1996 *Principles of Free-Electron Lasers*. London: Chapman and Hall.

[2] Conde, M. E. and Bekefi, G. 1991 *Phys. Rev. Lett.* **67**, 3082.

[3] Conde, M. E. and Bekefi, G. 1992 *IEEE Trans. Plasma Sci.* **20**, 240.

[4] Jha, P. and Kumar, P. 1996 *IEEE Trans. Plasma Sci.* **24**, 1354.

[5] Esmaeilzadeh, M., Mehdian, H. and Willett, J. E. 2002 *Phys. Rev.* E **65**, 016501.

[6] Friedland, L. 1980 *Phys. Fluids* **23**, 2376.

[7] Freund, H. P. and Drobot, A. T. 1982 *Phys. Fluids* **25**, 736.

[8] Esmaeilzadeh, M., Mehdian, H., Willett, J. E. and Aktas, Y. M. 2003 *Phys. Plasmas* **10**, 905.

[9] Caporasa, G. J., Rainer, F., Martin, W. E., Prono, D. S. and Cole, A. G. 1986 *Phys. Rev. Lett.* **57**, 1591.

[10] Ozaki, T., Ebihara, K., Hiramatsu, S., Kimura, Y., Kishuro, J., Monaka, T., Takayama, K. and Whittum, D. H. 1992 *Nucl. Instrum. Methods. Phys. Res.* A **318**, 101.